Journal of Sound and Vibration 329 (2010) 3709–3720

Contents lists available at ScienceDirect

Journal of Sound and Vibration

journal homepage: www.elsevier.com/locate/jsvi

Panel methods for airfoils in turbulent flow

Stewart A.L. Glegg [a], William J. Devenport [b,*]

[a] Florida Atlantic University, Ocean and Mechanical Engineering Department, Boca Raton, FL 33431, USA
[b] Virginia Tech, Aerospace and Ocean Engineering Department, 215 Randolph Hall, Blacksburg, VA 24061, USA

ARTICLE INFO

Article history:
Received 2 April 2009
Received in revised form
2 March 2010
Accepted 4 March 2010
Handling Editor: P. Joseph
Available online 24 April 2010

ABSTRACT

This paper describes how panel methods can be used to calculate the unsteady loading and radiated noise from airfoils in incompressible turbulent flow, while completely accounting for the mean flow distortion of the turbulence in the vicinity of the blade. Formulations based on the velocity and on the stagnation enthalpy are discussed. In three-dimensional flows, care must be taken with the velocity-based formulation to avoid singular behavior associated with vortex stretching by the mean flow. The velocity-based method is implemented in two dimensions to illustrate application of these methods, and is validated against Amiet's theory. Calculations showing the effect of blade thickness and angle of attack on the unsteady loading spectra are given. It is concluded that airfoil angle of attack has only a small effect on the unsteady loading, but that blade thickness reduces the spectral levels at high frequencies.

1. Introduction

The broadband noise from turbomachinery is often dominated by the effects of unsteady loading caused by the response of the blades to a turbulent inflow. This is referred to as leading edge noise. For example, this mechanism dominates broadband rotor stator interaction noise, and is also important for low speed fans. The prediction of leading edge noise in low speed fans is directly related to the unsteady loading on the fan blades, and so a clear understanding of how this is affected by airfoil thickness and angle of attack is important for the optimization of blade sections for low noise. In this paper we will consider the unsteady loading on airfoils and show how it may be predicted for blades of arbitrary shape using a panel method.

The use of time-domain boundary-element methods to calculate unsteady loading on airfoils is not new. There have been multiple studies that have considered this approach focusing on blade vortex interactions [1–4] and ducted rotors [5], for example. Many of these efforts have been based on the panel method formulation of Gennaretti et al. [6]. However, these studies have been concerned with the response to large coherent disturbances, such as those produced by mean flow distortions or tip vortices. They have not considered the statistical modeling required when a blade interacts with a turbulent inflow for which the disturbance is stochastic and the lengthscale is small relative to the chord.

When the unsteady inflow cannot be readily described by a simple flowfield, such as a compact vortex, most authors have instead opted to use a frequency domain analysis in which the incident disturbance is specified by a harmonic gust (for example, Refs. [7–12]). These studies have used both analytical and numerical methods to consider the effect of blade thickness and angle of attack on radiated noise, but only those which can be reduced to relatively simple analytical expressions [7,10,11] have been extended to turbulent inflow gusts. A discussion of the differences between the use of time

* Corresponding author. Tel.: +1 540 231 4456.
E-mail address: devenport@vt.edu (W.J. Devenport).

0022-460X/$ - see front matter © 2010 Elsevier Ltd. All rights reserved.
doi:10.1016/j.jsv.2010.03.007

domain boundary-element methods and analyses based on harmonic gusts is given by Grace [2], who concludes that boundary element methods have a number of advantages over harmonic gust approaches but that they are more difficult to apply to turbulent flows because of the problems of modeling the turbulent inflow with a set of discrete vortices.

In this paper it will be shown how this difficulty can be overcome, and how panel methods can be applied to blade turbulence interaction problems. The impact of mean flow distortion of turbulence on the accuracy of different panel methods will be discussed first, and then we will consider the specific application of panel methods to airfoils whose blade section does not vary with span. Results will be given for the unsteady loading on airfoils of different cross section and at different angles of attack and the calculations will be compared to the results of analytical methods.

2. The boundary value problem

Grace [2] used a two dimensional panel method to calculate the unsteady loading due to a blade vortex interaction. The formulation was based on the solution to Laplace's equation for the velocity potential with a boundary condition which required that the velocity induced by the vortex at the surface was canceled by the surface source distribution. The velocity field induced by the vortex was calculated from the Biot–Savart law, which implicitly assumes that the inflow disturbance is purely vortical. While this is appropriate for two dimensional problems, the extension of this approach to three dimensional problems needs to account for the stretching of the vorticity by the mean flow over the surface.

Goldstein [13] used the linearized Euler equations to formulate an equation for the perturbation velocity potential caused by an upstream vortical gust incident on a stationary body in a uniform mean flow, specified in the absence of the body as $\hat{\mathbf{i}}U_\infty$. For incompressible flow Goldstein gives

$$\nabla^2\phi' = -\nabla\cdot\mathbf{u}^{(I)}, \quad u_i^{(I)}(\mathbf{x},t) = (\partial X_j/\partial x_i)u_j^{(\infty)}(\mathbf{X}-\hat{\mathbf{i}}U_\infty t) \tag{1}$$

where $u_i^{(\infty)}(\mathbf{x})$ is the unsteady component of the vortical gust in the absence of the airfoil at time $t=0$, and location $\mathbf{x}$. The solution is given in terms of the drift coordinates $\mathbf{X}$, which are the solutions to the transport equation $\frac{D_o}{Dt}(\mathbf{X}-\hat{\mathbf{i}}U_\infty t)=0$.

The difficulty with this formulation is that the gradient of the drift coordinates $\partial X_j/\partial x_i$ is singular at the upstream stagnation point of the airfoil. Furthermore it is shown by Atassi and Grzedzinski [14] that $\mathbf{u}^{(I)}$ is undefined on the surface of a body downstream of the stagnation point, and so Eq. (1) is unsuitable for a boundary element or panel method solution. Atassi and Grzedzinski [14] propose that an additional potential ϕ^* is superimposed on the flow so that the boundary condition is $\nabla(\phi+\phi^*)+\mathbf{u}^{(I)}=0$ on the surface. This eliminates the singular solution on the surface but introduces additional boundary conditions on the upstream flow. Scott and Atassi [15] solve the modified version of Goldstein's equation using a finite volume method for a harmonic vortical gust. The extension of this approach to turbulent flows requires that the finite volume solution is calculated for all wavenumbers in the turbulence spectrum, which can be computationally intensive.

A boundary element method for incompressible unsteady flows can be obtained by using generalized derivatives as described by Howe [16]. We define the flow velocity $\mathbf{v}$ in the presence of a stationary surface specified by the function $f(\mathbf{x})=0$ (with $f<0$ inside the surface and $f>0$ outside the surface), and take the double curl of $H(f)\mathbf{v}$ where $H()$ is the Heaviside function, then for incompressible flow and an impermeable surface

$$\nabla\times\nabla\times(H(f)\mathbf{v}) = -\nabla^2(H(f)\mathbf{v}) = \nabla\times(H(f)\boldsymbol{\omega}+\mathbf{n}\times\mathbf{v}|\nabla f|\delta(f)) \tag{2}$$

where $\boldsymbol{\omega}$ is the vorticity and $\mathbf{n}$ the normal to the surface. Howe [16] gives the solution to this equation as

$$H(f)\mathbf{v}(\mathbf{x},t) = \nabla\times\int_{V_e}\frac{\boldsymbol{\omega}(\mathbf{y},t)}{4\pi|\mathbf{x}-\mathbf{y}|}\,dV(\mathbf{y}) + \nabla\times\int_S\frac{\mathbf{n}\times\mathbf{v}(\mathbf{y},t)}{4\pi|\mathbf{x}-\mathbf{y}|}\,dS(\mathbf{y}) \tag{3}$$

where V_e is the volume exterior to the surface S on which $f=0$. The first term represents the Biot–Savart law and gives the velocity induced by the vorticity in the flow. The second term gives the contribution from bound vorticity on the surface and can be evaluated using a vortex based panel method. The simplicity of this approach eliminates the need for assuming a potential flow and potential flow modeling of the airfoil wake. The incoming disturbance is completely specified in terms of its vorticity, and its evolution will be given by the solution to the vorticity equation. Finally the surface loading can be obtained by integrating the unsteady form of Bernoulli's equation over the blade surface and the wake.

This approach is well suited to two-dimensional flows where one is only considering the response of the airfoil to the spanwise component of the vorticity. As demonstrated below only this component need be considered to determine the overall unsteady lift or sound field. However, in three-dimensional applications, or when more detailed response information is required, the specification of the vorticity in Eq. (3) could be problematic because of stretching by the mean flow of non-spanwise components as they pass the blade. For example Fig. 1 shows a vertical line vortex as it passes an airfoil which has a thickness of 12%, assuming rapid distortion theory. The vortex line is never broken and so the vorticity closest to the surface continues to distort with time until the vortex tube becomes infinitely thin and lies on the surface. The vorticity increases with stretching and so the velocity induced at the surface by the stretched vortex will be very large and difficult to calculate numerically. One way of handling this problem would be to specify the incident vorticity field as a volume distribution of doublets, which can be discretized as point singularities rather than filaments (the curl of the doublet distribution represents the vorticity field).

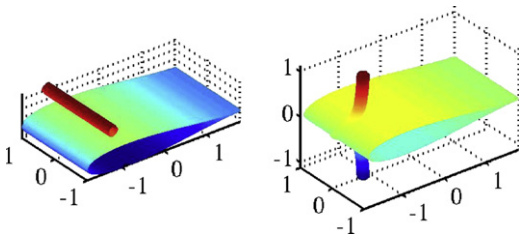

Fig. 1. Different types of blade vortex interactions for two dimensional flow over an airfoil.

An entirely different boundary element method can be formulated in terms of stagnation enthalpy by starting with Crocco's form of the momentum equation

$$\frac{\partial \mathbf{v}}{\partial t} + \nabla B + \boldsymbol{\omega} \times \mathbf{v} = 0 \tag{4}$$

where B is the stagnation enthalpy. All variables are a function of time t and their position $\mathbf{x}$. It is convenient to relate the stagnation enthalpy to a potential φ, and the local pressure p using

$$B = -\frac{\partial \varphi}{\partial t}, \quad \frac{\partial p}{\partial t} = \rho \frac{DB}{Dt} \tag{5}$$

Note that the potential φ is not the same as the conventionally defined velocity potential. However, if we can solve for the potential φ on the surface of the airfoil we can use Eq. (5) to obtain the local surface pressure, the unsteady loading and the radiated noise. Taking the divergence of Eq. (4) for an incompressible flow gives

$$\nabla^2 \dot{\varphi} = \nabla \cdot (\boldsymbol{\omega} \times \mathbf{v}) \tag{6}$$

A solution to this equation is obtained using a standard approach for a field in the presence of a stationary impermeable surface specified by the function $f(\mathbf{x})=0$ as

$$\dot{\varphi}(\mathbf{x}) H(f) = -\nabla \cdot \int_{V_e} \frac{\boldsymbol{\omega} \times \mathbf{v}}{4\pi |\mathbf{x}-\mathbf{y}|} dV(\mathbf{y}) - \nabla \cdot \int_S \frac{\dot{\varphi}(\mathbf{y}) \mathbf{n}}{4\pi |\mathbf{x}-\mathbf{y}|} dS(\mathbf{y}) \tag{7}$$

This method, in which the incident vorticity field is specified in terms of its Lamb vector $\boldsymbol{\omega} \times \mathbf{v}$, likewise works well for the case of spanwise vorticity interacting with a two-dimensional airfoil. However, it also is well suited to situations where it is necessary to consider other vorticity components or a three-dimensional mean flow. This is because the method elegantly removes the need to consider extended vortex filaments. Specifically, since vortex components parallel to the streamlines make no contribution to the stagnation enthalpy in Eq. (4) one can consider the flow generated by a disconnected vortex segment since such a segment can be imagined to be connected to infinity by filament arms that lie along the streamlines.

For the case of two-dimensional irrotational mean flow with three-component vorticity disturbances the Lamb vector $(\boldsymbol{\omega} \times \mathbf{v})_i$ simplifies considerably if rapid distortion theory is assumed. In this case the Lamb vector reduces to

$$\boldsymbol{\omega} \times \mathbf{v} \approx \boldsymbol{\omega} \times \mathbf{U} = (\boldsymbol{\omega} \cdot \hat{\mathbf{s}}) U \hat{\mathbf{z}} + \omega_3 U \hat{\mathbf{s}} \tag{8}$$

where $\hat{\mathbf{z}}$ and $\hat{\mathbf{s}}$ are orthogonal unit vectors in the spanwise direction and normal to the local flow velocity ($\hat{\mathbf{s}} = (\mathbf{U} \times \hat{\mathbf{z}})/U$), respectively.

The transport equation for the vorticity is given by the vorticity equation, which can be linearized about a potential mean flow to give

$$\frac{D_o \boldsymbol{\omega}}{Dt} - \boldsymbol{\omega} \cdot \nabla \mathbf{U} = 0 \tag{9}$$

The solution to Eq. (9) in terms of drift coordinates takes the form

$$\frac{\partial X_j}{\partial x_i} \omega_i(\mathbf{x}, t) = \omega_j^{(\infty)}(\mathbf{X} - \hat{\mathbf{i}} U^{(\infty)} t) \tag{10}$$

where $\omega_j^{(\infty)}$ is the vorticity in a volume V_T which lies well upstream of the blade in a region of uniform flow of mean velocity. The gradients of the drift functions X_2 and X_3 are given by

$$\nabla X_2 = \frac{U}{U_\infty} \hat{\mathbf{s}}, \quad \nabla X_3 = \hat{\mathbf{z}} \tag{11}$$

and so the Lamb vector can be evaluated using Eqs. (10) and (11) as

$$(\boldsymbol{\omega} \times \mathbf{U}) = U_\infty \omega_2^{(\infty)} \hat{\mathbf{z}} + U \omega_3^{(\infty)} \hat{\mathbf{s}} \tag{12}$$

The implication of the expansion in Eq. (12) is that the source in the volume integral of Eq. (7) is completely defined by the vorticity in the upstream region. The impact of vortex stretching is to increase the $\hat{\mathbf{s}}$ component of the Lamb vector in

proportion to the free stream velocity. Consequently the source term in Eq. (7) is never singular and can be specified in terms of the vorticity far upstream of the blade where the mean flow is uniform.

As mentioned above, only spanwise vorticity need be considered when computing the net unsteady loading from a two dimensional airfoil. To show this the net unsteady loading can be obtained from the spanwise integral of the unsteady pressure given by Eqs. (5) and (7). If we consider the integral of $\partial p/\partial t$ over the span we obtain

$$\begin{aligned}\rho\frac{D_o}{Dt}\int_{\text{span}}\dot{\varphi}(\mathbf{x})H(f)\,dx_3 = \rho\frac{D_o}{Dt}\Bigg\{&\int_{\text{span}}\int_{V_e}U_\infty\omega_2^{(\infty)}(\mathbf{X}(\mathbf{y})-\mathbf{U}^{(\infty)}t)\frac{(y_3-x_3)}{4\pi|\mathbf{y}-\mathbf{x}|^3}\,dV(\mathbf{y})\,dx_3\\&+\int_{span}\int_{V_e}U\omega_3^{(\infty)}(\mathbf{X}(\mathbf{y})-\mathbf{U}^{(\infty)}t)\frac{(\mathbf{y}-\mathbf{x})\cdot\hat{\mathbf{n}}}{4\pi|\mathbf{y}-\mathbf{x}|^3}\,dV(\mathbf{y})\,dx_3\\&+\int_{span}\int_{S}\dot{\varphi}(\mathbf{y})\frac{(\mathbf{y}-\mathbf{x})\cdot\hat{\mathbf{n}}}{4\pi|\mathbf{y}-\mathbf{x}|^3}\,dS(\mathbf{y})\,dx_3\Bigg\}\end{aligned}\tag{13}$$

For blades of infinite span for which end effects are negligible the first integral on the right hand side of Eq. (13) is zero because for each value of y_3 the integrand over x_3 is zero. The value of $\dot{\varphi}$ when integrated over the span will therefore only depend on the spanwise component of the vorticity. Hence the unsteady loading will also only depend on ω_3. This same result can be inferred starting with Eq. (3). The problem of modeling a turbulent inflow is therefore greatly simplified because only one component of the vorticity contributes to the unsteady lift and the unsteady loading on the blade can be calculated from the response of a two dimensional airfoil to the spanwise average of the spanwise vorticity component. This greatly simplifies the numerical cost of doing the calculation for the unsteady loading, which can be important for high frequency noise calculations, even for very simple systems.

3. Blade turbulence interactions

The problem of applying boundary element methods to turbulent flows [2] is greatly reduced by using the results of the analysis above. For blades of large span in a uniform mean flow we have shown that the unsteady loading can be calculated from the spanwise average of the spanwise vorticity component and the response to a two dimensional blade vortex interaction. In this section we will show how the response function can be coupled to the wavenumber spectrum of the upstream turbulence.

Following the approach used by Amiet [7], the unsteady loading caused by a turbulent inflow can be obtained from the response of the blade to a harmonic gust. In general the vorticity in the flow can be expressed in terms of its wavenumber transform in the region of flow far upstream of the blade where the flow is uniform:

$$\omega_3^{(\infty)}(\mathbf{x},t)=\int_{-\infty}^{\infty}\int_{-\infty}^{\infty}\int_{-\infty}^{\infty}a(k_1,k_2,k_3)e^{-ik_1(x_1-U_\infty t)-ik_2x_2-ik_3x_3}\,dk_1\,dk_2\,dk_3\tag{14}$$

Since the response is linear, the unsteady loading can be obtained by superimposing the response of the blade to harmonic gusts of amplitude $a(k_1,k_2,k_3)$. If the unsteady loading per unit span in response to a harmonic gust is denoted as $S(k_1,k_2,k_3)$, then the time history of the loading per unit span is

$$L_s(t,x_3)=\int_{-\infty}^{\infty}\int_{-\infty}^{\infty}\int_{-\infty}^{\infty}a(k_1,k_2,k_3)S(k_1,k_2,k_3)e^{ik_1U_\infty t-ik_3x_3}\,dk_1\,dk_2\,dk_3\tag{15}$$

The total unsteady loading is the integral of this over the span. For large spans this is well approximated as

$$L(t)=2\pi\int_{-\infty}^{\infty}\int_{-\infty}^{\infty}a(k_1,k_2,0)S(k_1,k_2,0)e^{ik_1U_\infty t}dk_1dk_2\tag{16}$$

and the loading in the frequency domain is

$$\tilde{L}(\omega)=\frac{2\pi}{U_\infty}\int_{-\infty}^{\infty}a(k_o,k_2,0)S(k_o,k_2,0)dk_2\tag{17}$$

with $k_o=-\omega/U_\infty$.

The procedure for calculating the far-field sound is to first use one of the methods outlined in Section 2 to do a series of calculations of the unsteady loading time history for a two dimensional blade in response to an elemental vortex introduced far upstream and convected past the blade. In each calculation the vortex is initiated at a different height x'_2 above the stagnation streamline, and the loading $L_v(t, x'_2)$ is calculated from the integration of the pressure around the blade. For the velocity-based formulation, the pressure is obtained from the unsteady Bernoulli equation, for the stagnation enthalpy formulation Eq. (5) is used. Such an elemental vortex of strength Γ has a vorticity initially described by the function

$$\omega_3^{(\infty)}(\mathbf{x},t)=\Gamma\delta(x_1-U_\infty t)\delta(x_2-x'_2)\tag{18}$$

and thus a wavenumber transform

$$a(k_1,k_2,0)=\frac{2R_3\Gamma}{(2\pi)^3}\exp(ik_2x'_2)\tag{19}$$

Substituting Eq. (19) into Eq. (16), we see that this vortex produces an unsteady loading

$$L_v(t,x_2') = \frac{2R_3\Gamma}{(2\pi)^2}\int_{-\infty}^{\infty}\int_{-\infty}^{\infty} S(k_1,k_2,0)e^{ik_1U_\infty t + ik_2x_2'}\,dk_1\,dk_2 \tag{20}$$

(where $2R_3$ is the blade span) which may be inverted to give

$$S(k_o,k_2,0) = \frac{U_\infty}{2R_3\Gamma}\int_{-\infty}^{\infty}\int_{-\infty}^{\infty} L_v(t,x_2)e^{i\omega t - ik_2x_2}\,dx_2\,dt \tag{21}$$

Hence, the numerical calculations of $L_v(t, x_2)$ can be used to obtain the blade response per unit span to a harmonic gust. (Note that in Ref. [20], Eq. 3, a multipying factor of 2π was added incorrectly and Eq. 21 gives the correction for this error.)

We next consider the unsteady loading spectrum which is defined as

$$S_{LL}(\omega) = \frac{\pi}{T}Ex[|\tilde{L}(\omega)|^2] = \frac{(2\pi)^2}{U_\infty^2}\int_{-\infty}^{\infty}\int_{-\infty}^{\infty}\frac{\pi}{T}Ex[a(k_o,k_2,0)a^*(k_o,k_2',0)]S(k_o,k_2,0)S^*(k_o,k_2',0)dk_2dk_2' \tag{22}$$

The turbulence is defined in a region of dimension $2R_1 \times 2R_2 \times 2R_3$ and the averaging time is $2T=2R_1/U_\infty$ we can simplify this integral using

$$\frac{\pi^2}{R_1R_3}Ex[a(k_o,k_2,0)a^*(k_o,k_2',0)] = \Omega_{33}(k_o,k_2,0)\delta(k_2-k_2') \tag{23}$$

where Ω_{33} is the wavenumber spectrum of the vorticity fluctuations. For isotropic homogeneous turbulence, Ω_{33} can be prescribed for a given lengthscale and turbulence intensity using the the three-dimensional energy spectrum function of the velocity fluctuations $E(k)$. As shown by Batchelor [17],

$$\Omega_{ij} = \frac{E(k)}{4\pi k^2}(k^2\delta_{ij}-k_ik_j) \tag{24}$$

where δ_{ij} is the Kronecker delta. Thus we have that $\Omega_{33}(k_o, k_2, 0)=E(k)/4\pi$ with $k=(k_o^2+k_2^2)^{1/2}$, and $E(k)$ is given for example by Amiet [7]. The final result is

$$S_{LL}(\omega) = \frac{4\pi R_3}{U_\infty}\int_{-\infty}^{\infty}\Omega_{33}(k_o,k_2,0)|S(k_o,k_2,0)|^2\,dk_2 \tag{25}$$

The far-field noise is calculated from the unsteady loading spectrum in the usual way giving, at a distance r from the blade, and at an angle θ to the direction of the loading, the sound spectrum as

$$S_{pp}(\omega) = (\omega\cos\theta/4\pi rc_o)^2S_{LL}(\omega) \tag{26}$$

where c_o is the speed of sound.

4. Numerical methods

4.1. Solving for the flow and sound

Two dimensional flow calculations were performed to illustrate the above methods using the velocity-based formulation governed by Eq. (3). Consider two dimensional flow in the x_1, x_2 plane containing vorticity $\boldsymbol{\omega}$ oriented in the x_3 direction, denoted by unit vector $\mathbf{e}_3$. In this case, the velocity on surface of the blade S, appearing in the last term in Eq. (3), is equal in magnitude to the bound vorticity per unit length of the blade surface $\gamma(\mathbf{y})$. The vector relationship between the two is $\mathbf{n}\times\mathbf{v}(\mathbf{y},t) = -\gamma(\mathbf{y})\mathbf{e}_3$. Making this substitution, and performing the curl operations on the right hand side of Eq. (3), we obtain

$$H(f)\mathbf{v}(\mathbf{x},t) = \int_{V_e}\frac{\boldsymbol{\omega}(\mathbf{y},t)\times(\mathbf{x}-\mathbf{y})}{4\pi|\mathbf{x}-\mathbf{y}|^3}\,dV(\mathbf{y}) - \int_S\frac{\gamma(\mathbf{y})\mathbf{e}_3\times(\mathbf{x}-\mathbf{y})}{4\pi|\mathbf{x}-\mathbf{y}|^3}\,dS(\mathbf{y}) \tag{27}$$

For a two dimensional mean flow Eq. (27) is first rewritten as

$$H(f)\mathbf{v}(\mathbf{x},t) = \int_{R_2}\int_{R_1}\int_{-\infty}^{\infty}\frac{\boldsymbol{\omega}(\mathbf{y},t)\times(\mathbf{x}-\mathbf{y})}{4\pi|\mathbf{x}-\mathbf{y}|^3}\,dy_3\,dy_1\,dy_2 - \oint_C\int_{-\infty}^{\infty}\frac{\gamma(\mathbf{y})\mathbf{e}_3\times(\mathbf{x}-\mathbf{y})}{4\pi|\mathbf{x}-\mathbf{y}|^3}\,dy_3\,ds(\mathbf{y}) \tag{28}$$

where R_1 and R_2 denote the extent of region V_e in the y_1, y_2 planes, C is the closed contour formed by the blade surface in this plane and ds is distance along that contour. Performing the integration in y_3 we obtain

$$H(f)\mathbf{v}(\mathbf{x},t) = -\int_{R_2}\int_{R_1}\frac{\boldsymbol{\omega}(\mathbf{y},t)\times(\mathbf{x}-\mathbf{y})}{2\pi|\mathbf{x}-\mathbf{y}|^2}\,dy_1\,dy_2 + \oint_C\frac{\gamma(\mathbf{y})\mathbf{e}_3\times(\mathbf{x}-\mathbf{y})}{2\pi|\mathbf{x}-\mathbf{y}|^2}\,ds(\mathbf{y}) \tag{29}$$

where $\mathbf{x}$ and $\mathbf{y}$ now represent the two-dimensional position vectors $(x_1, x_2, 0)$ and $(y_1, y_2, 0)$.

In theory a solution of Eq. (29) is straightforward. Since vorticity cannot be generated within the flow and must be convected in from the boundaries, the free vorticity $\boldsymbol{\omega}(\mathbf{y}, t)$ and the volume source it defines are known from the initial state and prior evolution of the flow. This vorticity is comprised of the incident vortex (introduced at the upstream flow

boundary or as part of the initial condition) and the vortex sheet convected into the domain from the blade trailing edge in response to fluctuations in the blade circulation produced by the interaction with that incident vortex. The bound vortex sheet strength $\gamma(\mathbf{y})$ can be determined from the non-penetration condition; that is, as the solution to the integral equation formed by evaluating Eq. (29) at the blade surface and setting its normal component to zero. Applying the Kutta condition (requiring that $\gamma(\mathbf{y})$ be zero at the trailing edge) and the Kelvin condition (requiring that the total circulation in the flow remains constant) ensures that this solution is unique.

In practice the above solution procedure must be performed numerically. Changes with time are discretized into intervals Δt and the free vorticity is represented as a sum of discrete elemental vortices of the form

$$\boldsymbol{\omega}(\mathbf{y},t)=\sum_m \Gamma_m \mathbf{e}_3 \delta(y_1-y_1^{(m)}(t))\delta(y_2-y_2^{(m)}(t)) \tag{30}$$

where Γ_m is the circulation of each elemental vortex, and $\mathbf{y}^{(m)}(t)$ its position. With this Eq. (29) becomes

$$H(f)\mathbf{v}(\mathbf{x},t)=-\sum_n \frac{\Gamma_n \mathbf{e}_3 \times (\mathbf{x}-\mathbf{y}^{(n)}(t))}{2\pi|\mathbf{x}-\mathbf{y}^{(n)}(t)|^2}+\oint_C \frac{\gamma(\mathbf{y})\mathbf{e}_3 \times (\mathbf{x}-\mathbf{y})}{2\pi|\mathbf{x}-\mathbf{y}|^2}\,ds(\mathbf{y}) \tag{31}$$

so that the velocity produced by each of the elemental vortices is given by the two-dimensional Biot–Savart law. Note the strengths of all the free-elemental vortices, except the one most recently shed from the blade trailing edge, will be known from the previous time step.

The blade surface is discretized into a polygon with N vertices $\mathbf{y}^{(n)}$ and the variation of vortex sheet strength around that surface is discretized as a piecewise linear function with values γ_n at the vertices (i.e. a classical linear vortex panel method, see Katz and Plotkin [18] for example). The surface integration can be performed analytically over each polygon side (or 'panel'), simplifying the integral over the contour C into a sum of these N results. With these simplifications, the integral equation for the boundary condition becomes an algebraic expression containing the N unknown vortex sheet strengths γ_n. These are determined together and the strength of the most recently shed wake vortex. The $N+1$ constraints needed are obtained from the Kutta condition, the Kelvin condition and by enforcing the non-penetration condition at the center point of all but one of the panels (the condition on the remaining panel being redundant).

The instantaneous lift per unit span is determined at each time step by integrating the pressure on the blade surface determined through the unsteady Bernoulli equation, i.e.

$$L=-\oint_C p\,dx_1=\frac{1}{2}\rho\oint_C |\mathbf{v}|^2\,dx_1+\rho\oint_C \frac{\partial\phi}{\partial t}\,dx_1 \tag{32}$$

where ϕ is the conventionally defined velocity potential. This is most easily calculated directly from the vortex sheet strength as

$$L=\frac{1}{2}\rho\oint_C \gamma^2\,dx_1+\rho\frac{\partial}{\partial t}\oint_C\int_0^s \gamma(s')\,ds'\,dx_1 \tag{33}$$

where all integrals are taken around the blade surface contour.

To complete the sound calculation, the unsteady lift calculated at discrete time intervals and discrete incident vortex positions x'_2 is numerically transformed in time and x'_2, according to Eq. (21), and then numerically integrated with the turbulent vorticity spectrum, as per Eq. (25).

4.2. Implementation

Mean flow and unsteady calculations are performed separately. The mean flow calculation, performed first, is integrated to determine the streamline pattern and drift functions. These define the convection paths and timing of the incident and shed vorticity in the unsteady calculation. The unsteady calculation is then performed repeatedly to obtain the linear perturbations to this solution produced by a series of weak discrete vortices initiated at different heights above the stagnation streamline and convected past the blade. A vortex strength of $10^{-4}U_\infty c$ was found to be sufficiently weak to provoke only a linear response. The unsteady calculation involves the shedding and convection of discrete vortices from the trailing edge. A new shed vortex is created just downstream of the trailing edge at each time step. The strength of this vortex is treated as unknown and solved for along with the panel strengths for that time step, the additional constraint being provided by the Kelvin condition.

Vortex trajectories that come close to the surface are important for computing the high frequency response of the blade but must be handled with care. If the distance between the vortex and the airfoil surface becomes less than a few panel lengths, the solution can oscillate wildly as the vortex passes over one panel to the next. Refining the entire paneling to avoid this is not practical, given that vortex trajectories passing as close as 0.05% chord from the airfoil surface are of interest. A far better solution is to adaptively refine the paneling in the vicinity of the vortex so as to ensure a panel size that is always small compared to the vortex/surface separation. The algorithm used in the present calculations was set to locally subdivide the baseline paneling to ensure panel sizes never less than one-fifth of the distance to the vortex. The use

of such an algorithm has the added benefit of making the calculation fairly insensitive to the density of the baseline paneling.

Near-surface vortex trajectories can also cause problems in their interaction with the trailing edge. As shown by Glegg and Devenport [19] this interaction should produce a singularity in the response that is exactly canceled by the Kutta condition. In the panel method, however, the cancelation is usually not perfect. The residual spike can result in some scalloping of the computed airfoil response function and predicted sound spectrum. This effect can be minimized by using panels of a constant length in the trailing edge region, by using a low-order representation of the wake (hence the present use of discrete wake vortices rather than panels) and by adjusting the distance downstream of the trailing edge where the new shed vortex appears (between 20% and 30% of the free-stream convection distance in one time step). Also, an effective post-processing technique is to simply replace the spike with loading values interpolated from the surrounding time history – an approach justified by the slow variation of the remainder of the loading history in this region.

The preferred discretization for the numerical calculation was as follows. Airfoil shapes were represented using a total of 200 panels with panel lengths varying from 0.1%c at the trailing and leading edges to 3.2%c near mid-chord. Mean streamline integrations were carried out using a predictor corrector algorithm with a time step of typically $0.01U_\infty/c$ except near the leading edge of the airfoil where this resolution is insufficient (particularly for thin airfoils at angle of attack). It was found that using steps of $0.0002U_\infty/c$ within 5% chord of the leading edge resulted in consistent streamline patterns even for the thinnest airfoils, without excessive computation time. For the unsteady part of the calculation, the incident vortex released 10 chords upstream of the leading edge, and allowed to convect over a total time period of $20U_\infty/c$ in even time steps of $0.01U_\infty/c$. The unsteady loading for 200 different incident vortex locations, from $x_2=-5c$ to $x_2=5c$, was computed. Locations in x_2 were not evenly spaced but concentrated around the stagnation streamline in a parabolic distribution, with the smallest positive and negative x_2 locations being $\pm 0.0005c$ (for flat plate calculations) and $\pm 0.002c$ for the Joukowski airfoil calculations. Results were then Fourier transformed and used to calculate the unsteady lift spectrum and far-field sound, as detailed above. The Fourier transform necessitated an interpolation in x_2 which was performed in steps of $0.005c$. Windowing of the lift response function before the Fourier transform was used to eliminate abrupt transitions at the calculation limits. A Chebychev window was used, but the exact form of the window was found to be unimportant with Blackman, Hanning and Tukey windows producing indistinguishable results.

5. Results

Extensive calculations were performed to examine the convergence behavior and establish the range of validity for broadband sound predictions made using the above numerical method. Many of these calculations were performed on a flat plate (numerically approximated as a 0.1% thick NACA 00XX airfoil) at zero angle of attack, because of the availability of the exact analytical solution of Amiet [7] for this case. Calculations were also performed on a 12% thick symmetric Joukowski airfoil, showing the effects of angle of attack. All calculations present sound levels as they would be heard by an

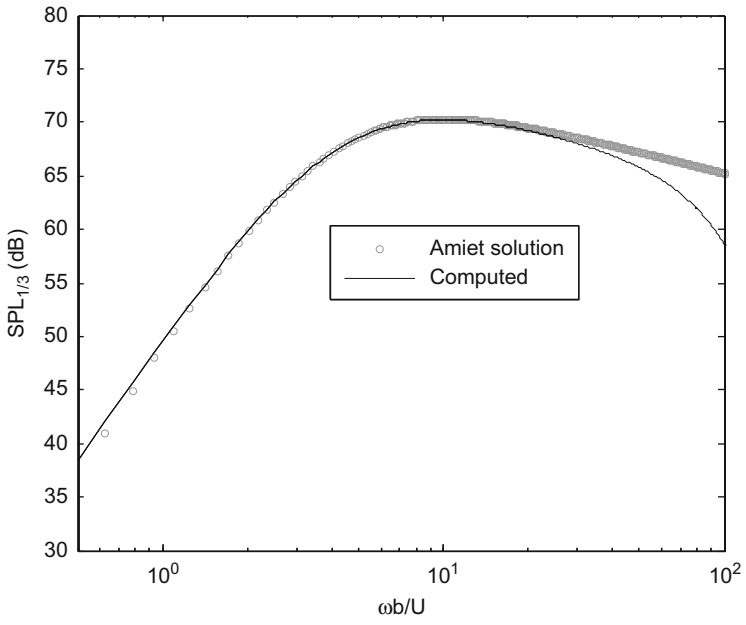

Fig. 2. Sound pressure level predicted using the vortex panel method compared with the exact analytical solution of Amiet for a flat plate at zero angle of attack with an integral scale $L/c=0.09$.

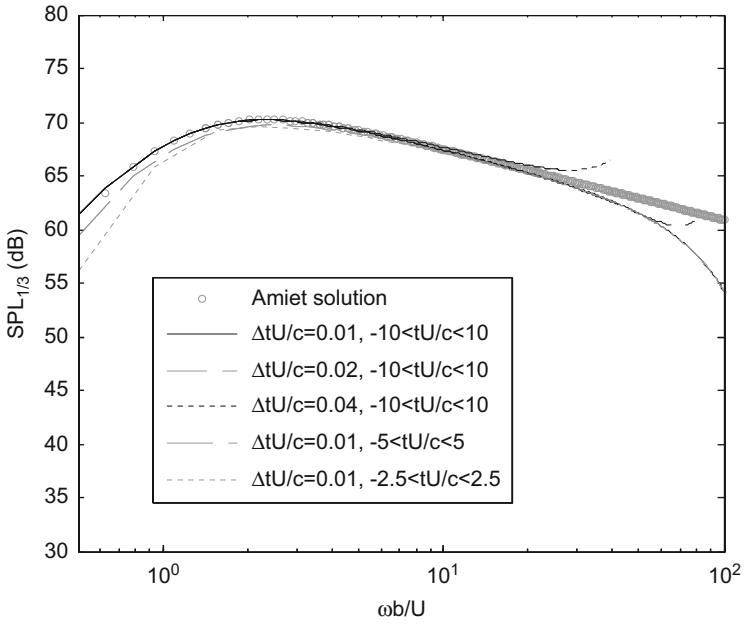

Fig. 3. Sound pressure level predicted using the vortex panel method compared with the exact analytical solution of Amiet for a flat plate at zero angle of attack with an integral scale L/c=0.4. Different curves show the effects of varying the time range and resolution of the calculation from the preferred values, represented by the solid black line.

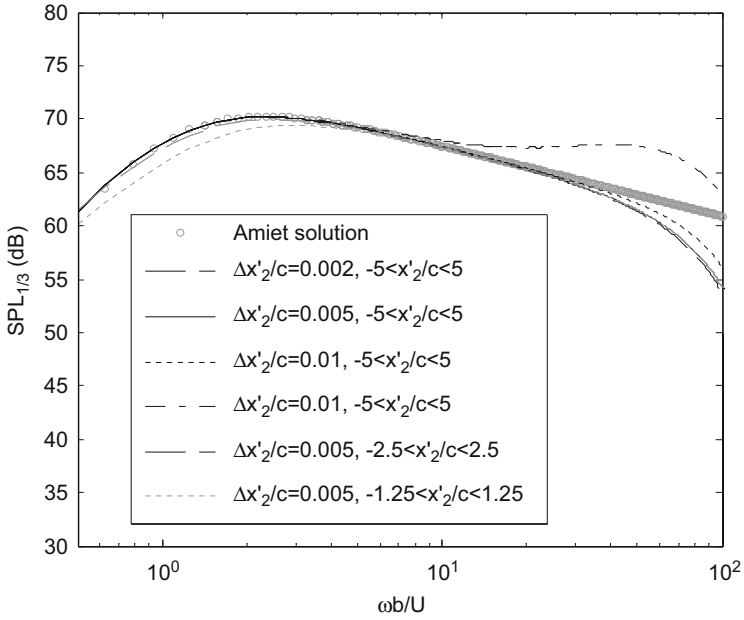

Fig. 4. Sound pressure level predicted using the vortex panel method compared with the exact analytical solution of Amiet for a flat plate at zero angle of attack with an integral scale L/c=0.4. Different curves show the effects of varying the x_2 range and resolution of the calculation from the preferred values, represented by the solid black line.

observer 1.8 m above the midspan of a 0.2-m chord, 1.8-m span blade immersed in a 30 m/s flow containing isotropic turbulence with an intensity of 3.9%. Results are presented for integral scale to chord ratios of 0.09 and 0.4.

Broadband noise spectra for the flat plate are plotted in Figs. 2 and 3 in terms of 1/3rd octave band sound pressure level referenced to 20 μPa. Compared with Amiet's analytical solution the predictions appear accurate up to quite high reduced frequencies where the computed sound levels start to fall below those of the exact result. For both integral scales, computed sound levels are within 1 dB of the correct values up to ω_r=40, and 2 dB up to ω_r=60.

The departure of the computed from the theoretical curves raises the question of convergence – i.e. the extent to which the computed spectra depend upon the chosen discretization detailed above. This was examined through a series of repeated calculations of the larger integral scale case, the results of which are presented in Figs. 3–6. Fig. 3 shows the dependence of the solution on the overall time range of the simulations T ($-T<t<T$) and the time step size Δt. The time range affects the low frequency part of the spectrum, which clearly converges with Amiet's solution with $TU_\infty/c=10$. The time step size affects high frequency spectral levels which converge at least up to $\omega_r=60$ for $\Delta t U_\infty/c=0.02$. Note that the

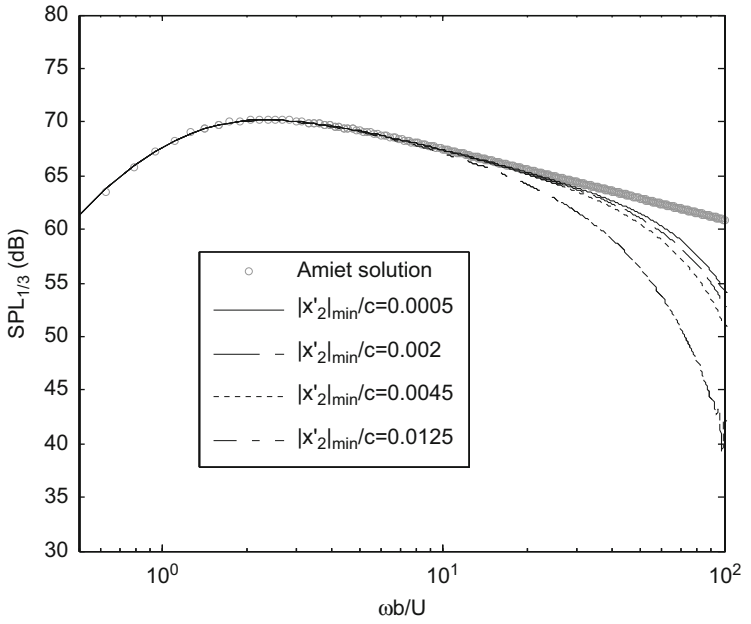

Fig. 5. Sound pressure level predicted using the vortex panel method compared with the exact analytical solution of Amiet for a flat plate at zero angle of attack with an integral scale $L/c=0.4$. Different curves show the effects of varying how close to the stagnation streamline the vortices are released, from the preferred value represented by the solid black line.

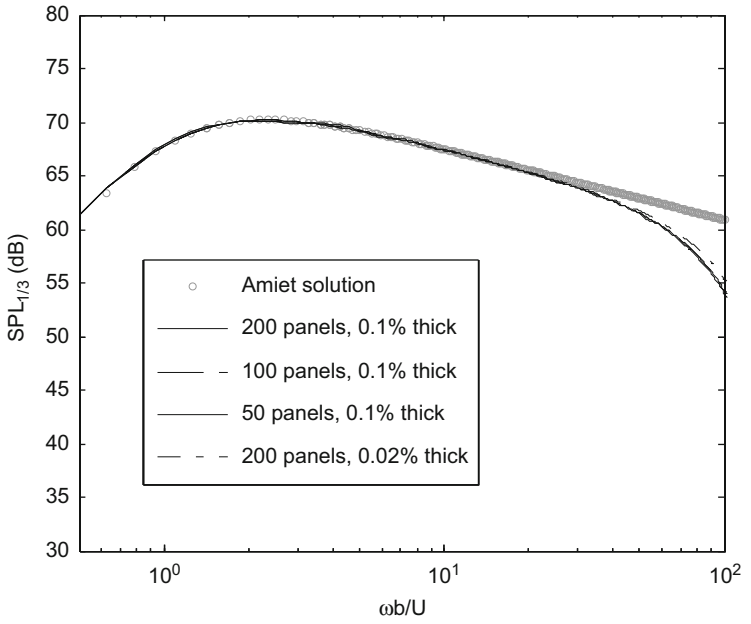

Fig. 6. Sound pressure level predicted using the vortex panel method compared with the exact analytical solution of Amiet for a flat plate at zero angle of attack with an integral scale $L/c=0.4$. Different curves show the effects of varying the number of panels (from the preferred value of 200) and of using a different maximum plate thickness.

convergence here is not to Amiet's solution, indicating that the time step is not responsible for the high-frequency roll of in the computed spectrum. Fig. 4 shows the dependence of the solution on the overall range of initial vortex positions X'_2 ($-X'_2 < x'_2 < X'_2$) and the step size of the interpolation of the lift response function $\Delta x'_2$. An X'_2 of 5 chordlengths is clearly enough for the low-frequency sound spectrum to converge to Amiet's solution, whereas a $\Delta x'_2$ of 0.5% chord is enough for convergence at high frequencies though, again, this is clearly not the source of the high frequency roll off. Fig. 5 shows the dependence of the solution on how close to the stagnation streamline the vortices are released (i.e. $|x'_2|_{\min}$). The high-frequency part of the spectrum converges towards the Amiet solution as this distance is reduced. For $|x'_2|_{\min}$ less than 0.5%

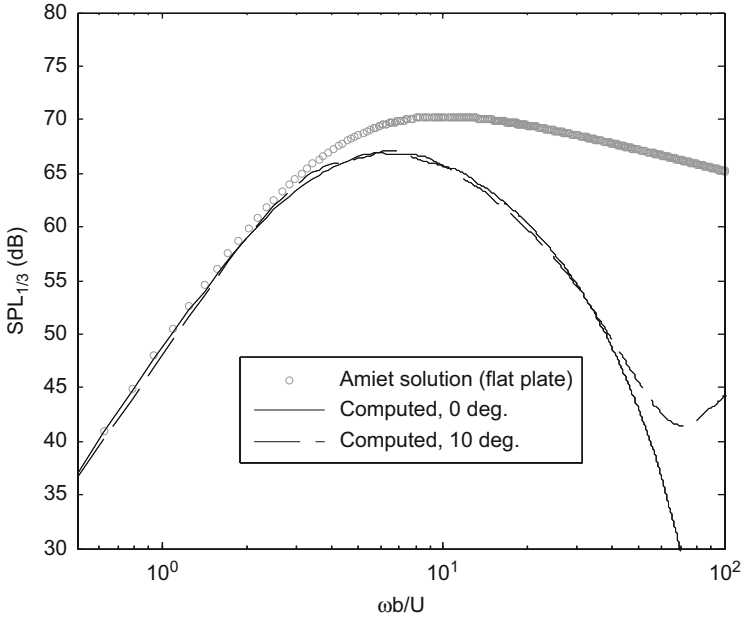

Fig. 7. Sound pressure level for a 12% thick symmetric Joukowski airfoil predicted using the vortex panel method for 0° and 10° angle of attack compared with Amiet's flat-plate theory with L/c=0.09.

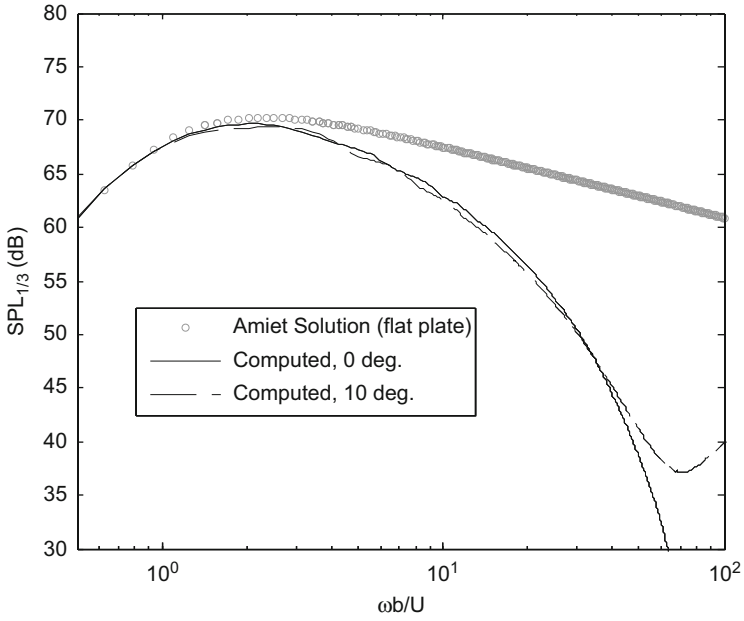

Fig. 8. Sound pressure level for a 12% thick symmetric Joukowski airfoil predicted using the vortex panel method for 0° and 10° angle of attack compared with Amiet's flat-plate theory with L/c=0.40.

chord, however, the rate of change is quite small and, while not fully converged, there is almost no significant difference between the sound spectra calculated with an $|x'_2|_{\min}$ of 0.2% and 0.05% chord. Fig. 6 shows the calculation to be completely independent of the number of panels used to represent the plate, at least down to 50 panels. This figure also shows a calculation performed with the maximum plate thickness reduced from 0.1% to 0.02% chord. We see that the finite thickness of the plate in the computations has a small but observable effect in limiting the high-frequency range of the calculation.

To show the effect of angle of attack and blade thickness on the radiated noise, calculations were carried out for a 12% thick Joukowski foil at angle of attack of 0° and 10°. The results are shown in Figs. 7 and 8 for the two integral scale to chord ratios. The effects of angle of attack are very small for reduced frequencies below 40, where the calculation should be fully converged. However, the effect of blade thickness is to reduce the spectral level at middle and high frequencies by a large amount. This result is consistent with the analytical results and Howe [10], Gerschfeld [11] and Glegg and Devenport [19]. The physical mechanism for these effects is given by Glegg and Devenport [19] who show that the effect of angle of attack on the response of an airfoil to a symmetric gust is to rotate the direction of the unsteady loading vector without altering its magnitude. The numerical results shown in Figs. 7 and 8 confirm this finding. The analytical results show that the effect of increasing the blade thickness is to smooth the blade response as the gust passes the leading edge of the airfoil, and this reduces the high frequency content of the loading noise, as indicated in Figs. 7 and 8.

6. Conclusions

The prediction unsteady loading and sound radiation from an airfoil in incompressible turbulent flow using panel methods has been discussed. Solution of the fundamental governing equations reveals two distinct approaches. The first resembles a conventional vortex panel method in which the Biot–Savart law is used to solve for the flow velocity induced by incident vorticity. In the second approach a velocity potential is defined in terms of the stagnation enthalpy. In this case the influence of the incident vorticity is given in terms of its Lamb vector $\boldsymbol{\omega} \times \mathbf{v}$. Both methods are well suited to finding the two-dimensional blade response function but in three-dimensional problems, vortex stretching in the vicinity of stagnation points may cause numerical problems for a velocity-based approach. Such problems would not occur in the stagnation enthalpy approach; however, because it is not necessary to consider extended vortex filaments.

The problem of the sound produced by a real airfoil is considered. It is shown that this simplifies so that only the spanwise average of the spanwise component of the inflow vorticity need be considered. This can be obtained using a purely two dimensional blade response calculation.

A panel method code has been developed to examine the practicability and accuracy of sound calculations made using this approach. The method is two dimensional and only considers the response to spanwise incident vorticity. However, in a major simplification it is shown that only this need be considered for the case of a two-dimensional blade immersed in 3-dimensional homogeneous turbulence. The panel method is shown to produce well resolved sound predictions up to a reduced frequency of about 40. Sample calculations with the method show that airfoil thickness substantially attenuates the high frequency content of radiated noise and that, at least for a 12% thick airfoil in isotropic turbulence, the noise spectrum is almost independent of angle of attack.

Acknowledgements

This work was sponsored by the Office of Naval Research through Grants N00014-05-1-0463 and N00014-05-1-0464, and the authors would like to thank Dr. Ron Joslin for his encouragement and support for this work.

References

[1] D. Rockwell, Vortex body interactions, *Annual Review of Fluid Mechanics* 30 (1998) 199–229.
[2] S.M. Grace, unsteady blade response: the BVI model vs. the gust model, *Proceedings of the Seventh AIAA/CEAS Aeroacoustics Conference*, Maastricht, AIAA Paper no. 2001-2209, 2001.
[3] M. Gennaretti, G. Bernadini, Novel boundary integral formulation for blade–vortex interaction aerodynamics of helicopter rotors, *AIAA Journal* 45 (2007) 1169–1176.
[4] C. Testa, S. Ianniello, F. Slavatore, M. Gennaretti, Numerical approaches for hydroacoustic analysis of marine propellers, *Journal of Ship Research* 52 (2008) 57–70.
[5] E. Quaranta, D. Drikakis, Noise radiation from a ducted rotor in a swirling-translating flow, *Journal of Fluid Mechanics* 641 (2009) 463–473.
[6] M. Gennaretti, L. Luceri, L. Morino, A unified boundary integral methodology for aerodynamics and aeroacoustics, *Journal of Sound and Vibration* 200 (1997) 467–489.
[7] R.K. Amiet, Acoustic radiation from an airfoil in a turbulent stream, *Journal of Sound and Vibration* 41 (1975) 407–420.
[8] H.M. Atassi, The Sears problem for a lifting airfoil revisited new results, *Journal of Fluid Mechanics* 141 (1984) 109–122.
[9] M.R. Myers, E.J. Kerschen, Influence of incidence angle on sound generation by airfoils interacting with high frequency gusts, *Journal of Fluid Mechanics* 292 (1995) 271–304.
[10] M.S. Howe, Correlation of lift and thickness noise sources in vortex airfoil interactions, *Journal of Sound and Vibration* 137 (1990) 1–7.
[11] J. Gershfeld, Leading edge noise from thick airfoils in turbulent flows, *Journal of the Acoustical Society of America* 116 (2004) 1416–1426.
[12] D.P. Lockard, P.J. Morris, Radiated noise from airfoils in realistic mean flows, *AIAA Journal* 36 (1998) 907–914.

[13] M.E. Goldstein, Unsteady vortical and entropic distortions of potential flows around arbitrary obstacles, *Journal of Fluid Mechanics* 89 (1978) 433–468.
[14] H.M. Atassi, J. Grzedzinski, Unsteady disturbances of streaming motions around bodies, *Journal of Fluid Mechanics* 209 (1989) 389–403.
[15] J.R. Scott, H.M. Atassi, A finite difference frequency domain numerical scheme for the solution of the gust response problem, *Journal of Computational Physics* 119 (1995) 75–93.
[16] M. Howe, *Acoustics of Fluid–Structure Interaction*, Cambridge University Press, 1998.
[17] G.K. Batchelor, *The Theory of Homogeneous Turbulence*, Cambridge University Press, 1953.
[18] J. Katz, A. Plotkin, *Low Speed Aerodynamics*, second ed, Cambridge University Press, 2000.
[19] S. Glegg, W. Devenport, Unsteady loading on an airfoil of arbitrary thickness, *Journal of Sound and Vibration* 319 (2009) 1252–1270.
[20] W.J. Devenport, J.K. Staubs, S.A.L. Glegg, Sound radiation from real airfoils in turbulence, Journal of Sound and Vibration (2010), doi:10.1016/j.jsv.2010.02.022.